Anisotropic Stiffness Effect on Stability of a Magnetically Suspended Momentum Wheel

K. Tsuchiya* and M. Inoue†
Mitsubishi Electric Corporation, Amagasaki, Hyogo, Japan
S. Akishita‡
Ritsumeikan University, Kita-ku Kyoto, Japan
A. Nakajima§ and Y. Ohkami¶
National Aerospace Laboratory, Chofu, Tokyo, Japan
and
C. Murakami**
Tokyo Metropolitan Institute of Technology, Hino, Tokyo, Japan

This paper describes a method for designing the bearing stiffness and analyzing the damping characteristics of the whirling motion of a momentum wheel that is actively stabilized in the axial direction and passively supported in two orthogonal radial directions by magnetic force. A method for estimating the magnetic bearing stiffness is introduced, which uses magnetic circuit theory and numerical simulation technique. The equations of rotor motion include the effect of anisotropic stiffness of bearing. A solution to the equations of motion is obtained by applying the method of averaging, relating the relationship of the damping characteristics variation with angular speed to the anisotropy of stiffness. The limiting speed, where the damping factor is equal to null, increases by the quantity proportional to the difference of the bearing stiffness in two orthogonal directions perpendicular to the axis of rotation. The result was verified by the experiment with a single-axis controlled and magnetically suspended momentum wheel.

Introduction

MAGNETICALLY suspended momentum wheels in spacecraft attitude control systems offer several advantages over a ball bearing wheel. These advantages include friction-free rotation, reduction of energy consumption, long lifetime, and high reliability. The use of such a wheel in a bias momentum attitude control system provides very remarkable benefits such as high precision control and long lifetime. Five types of magnetic suspension utilizing attractive force between stator and rotor can be categorized according to the actively controlled degrees of freedom.[1] Each type has its own advantages and disadvantages. Generally speaking, complexity in the control circuit increases with the number of the actively controlled degrees of freedom (hereafter referred to as "axis"). This increase results inevitably in an increase of power consumption and deterioration in reliability of the bearing system. Of the five types, the single-axis controlled magnetic suspension system has attracted the most attention due to its simplicity and possibilities for high-speed wheels. Some models of single-axis control systems, which were developed in Europe, have been reported.[2,3]

Figure 1a shows schematically a single-axis controlled wheel. Active control is applied in the axial suspension of the rotor, and passive stabilization works in the two radial axes by the attractive force generated by the permanent magnet. One way to sustain the stability of the motion of this type of rotor is to increase the radial bearing stiffness. We can obtain a high critical speed of rotor by using high bearing stiffness. An efficient design method is achieved by applying the theory of magnetism. Another efficient way is to increase the damping factor of the rotor dynamic motion. High rotational speed beyond the critical speed can be attained with the high damping factor. It is well known that internal dissipation in the rotor causes instability of the radial whirling motion at such high rotational speed.[4,5] In this paper, we develop analytical expressions for the increase of the damping factor due to anisotropy in radial bearing stiffness. The uniqueness of our method is the transfer of structural anisotropy in the stator into the bearing stiffness anisotropy.

The angular speed of the isotropic bearing where the damping factor decreases to null, called "limiting speed," depends on the ratio of the stator damping factor vs the rotor damping factor and the critical speed. On the other hand, the limiting speed of the anisotropic bearing depends on the difference of the bearing stiffness. By making a difference in the bearing stiffness in two orthogonal transverse directions, the limiting speed of the rotor can be increased remarkably. It is found that one way to make a difference in bearing stiffness along two radial axes is to introduce structural anisotropy into the stator.

In this paper, the design method of stiffness of single-axis controlled magnetic bearing is described first. The way of increasing the magnetic bearing stiffness and the correct estimation of the stiffness are discussed. Second, the dynamic behavior of a rotor supported by single-axis controlled magnetic bearing is analyzed. An expression relating the limiting speed of the rotor and the bearing stiffness is deduced. Experimental results verifying the effectiveness of the analysis are also presented.

Designing a Method for Determining Bearing Stiffness

In this section the method for determining the load-carrying capacity of single-axis controlled magnetic bearing is de-

Presented as Paper 89-0545 at the AIAA 27th Aerospace Science Meeting, Reno, NV, Jan. 9–12, 1989; received Jan. 26, 1989; revision received March 6, 1990.

*Senior Research Engineer, currently Professor, Osaka Univ.
†Research Engineer.
‡Professor. Member AIAA.
§Senior Researcher.
¶Senior Researcher. Member AIAA.
**Professor.

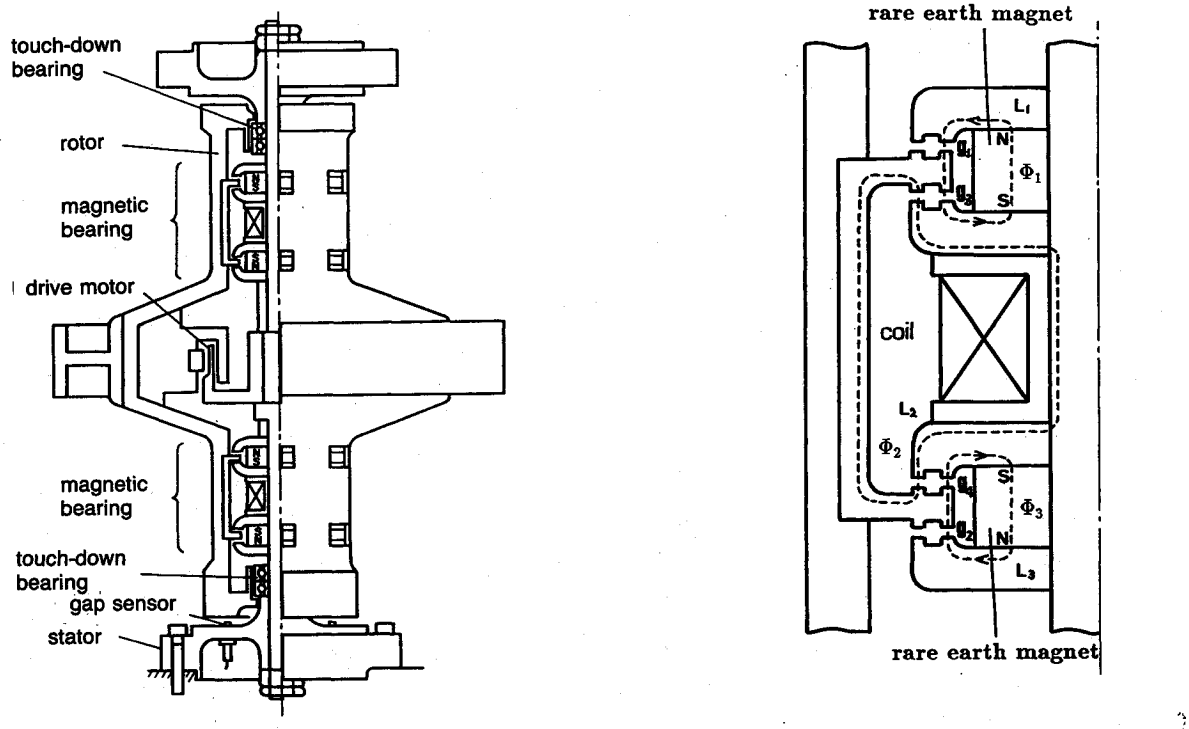

a) Schematic configuration

b) Magnetic path in magnetic bearing

Fig. 1° Configuration of single-axis controlled magnetic bearing wheel.

scribed. As already discussed, high bearing stiffness is necessary to attain high rotational speed of the wheel. The high bearing stiffness can be realized with precise estimation of the bearing characteristics.

Preceding the discussion of the method, we shall explain the principal construction of the wheel. As shown in Fig. 1a, a pair of the magnetic bearings are located in a longitudinal symmetric position. A pair of coils excite a modulated magnetic field that is applied to actively control the axial motion of the rotor. The gap sensors of eddy current type are located on the lowermost part, and the rotor position signal is fed to the feedback controller. A pair of touchdown ball bearings, in both the uppermost and the lowermost parts, work effectively only when the magnetic bearing does not work. They prevent the rotor from touching down impulsively to the stator teeth due to the action of the permanent magnet.

Virtually zero power control[6] was introduced into our model in order that the energy consumption in the control system should be minimized. As shown in Fig. 1b, three closed magnetic flux lines are formed in each of the upper and lower magnetic bearings in our model. The magnetic flux in the upper and lower magnetic paths, L_1 and L_3, is generated by only the rare-earth permanent magnet. The magnetic flux of the middle path, L_2, is generated by the control current of the coil and applied to stabilize the axial motion of the wheel rotor. The magnetic field that is needed to hold the rotor against an external stationary force in a position between the magnetic poles of the stator is generated by each of the two pieces of the rare-earth magnet. Therefore, the procedure for estimating the load-carrying capacity in the nominal condition is preceded by the other. In Fig. 1b the gaps and the magnetic paths of the bearing form an axisymmetrical configuration at the nominal condition of equilibrium. The clearances from top to bottom of the four gaps are defined as g_1, g_3, g_4, and g_2, respectively. The magnetic fluxes of the three closed paths are defined as Φ_1, Φ_3, and Φ_2, respectively, as shown in Fig. 1b.

Using the analogy between magnetic and electric circuits where magnetic flux Φ is compared with electric current, reluctance R with resistance, and magnetomotive force E_m with electromotive force, the magnetic flux Φ_1 in the magnetic path L_1 is represented by

$$(R_1 + R_3 + r)\Phi_1 = E_m \tag{1}$$

where R_1 and R_3 are the reluctance in the gap g_1 and the gap g_3, respectively, E_m is the magnetomotive force in the rare-Earth permanent magnet, and r is the internal reluctance in the permanent magnet. The magnetomotive force E_m is related to the demagnetization H_c of the permanent magnetic:

$$E_m = l_m H_c \tag{2}$$

where l_m is the length of the path along the principal magnetic field in the permanent magnet. The internal reluctance r is expressed by

$$r = \mu_0(A_m/l_m) \tag{3}$$

where μ_0 is the magnetic permeability of free space and A_m is the cross-sectional area of the permanent magnet along the principal magnetic field.

Reluctances R_1 and R_3 in the gap are influenced by the flux leakage. A numerical simulation technique for magnetic fields was applied in the computation of those in the vicinity of the gap. From the computation it was found that the flux leakage was governed by the dimensions and the configuration of the teeth in the gap. The precise distribution of the efficient flux may be obtained by the numerical simulation technique. However, a simple and convenient technique is more advantageous in designing estimation. So, applying Roters' method,[7] the reluctance R_1 in the gap g_1 and the reluctance R_3 in the gap g_3 are represented by the following equations considering the effect of the leaked flux:

$$R_1 = \frac{l_{g1}}{\mu_0 A_1(1+\alpha_1\alpha_2)}\left(1 - \frac{\alpha_1 + \alpha_0\alpha_2}{1+\alpha_1+\alpha_2}\frac{z_1}{l_{g1}}\right) \tag{4}$$

$$R_3 = \frac{l_{g3}}{\mu_0 A_3(1+\alpha_1\alpha_2)}\left(1 - \frac{\alpha_1 + \alpha_0\alpha_2}{1+\alpha_1+\alpha_2}\frac{z_3}{l_{g3}}\right) \tag{5}$$

where A_1 and A_3 are the cross-sectional areas of the teeth, and l_{g1} and l_{g3} the gap clearance lengths, respectively, in the gap g_1 and the gap g_3 ; α_0, α_1, and α_2 are nondimensional coefficients depending on the configuration of the teeth. In these equations, the influence of the small displacement z_1 and z_3 ($\ll l_{g1}$ and l_{g3}) are expressed in the second terms in the right side parentheses. Using Eqs. (1-5), we can estimate the magnetic flux Φ_1 of a round of the loop. The magnetic flux density, for example, B_j in the gap g_j, is deduced as

$$B_j = \frac{\Phi_j}{A_j}\frac{1}{f_j} \qquad (j = 1,3) \tag{6}$$

where $1/f_j$ is the effective flux ratio to the total flux representing the stiffness of the attractive force; it is represented approximately by

$$\frac{1}{f_j} \cong \frac{1}{1+\alpha_j+\alpha_2}\left(1+\frac{1+\alpha_j-\alpha_0}{1+\alpha_j+\alpha_2}\right) \qquad (j = 1,3) \tag{7}$$

The axial magnetic suspension force F_a is estimated as

$$F_a = (1/2\mu_0)(A_1B_1^2 + A_3B_3^2) \tag{8}$$

From F_a, we can obtain an approximate axial bearing stiffness k_a by using the equation $k_a = \partial F_a/\partial z$. Assuming $z_1 = z_3 = z$, $A_1 = A_3 = A$, and $l_{g1} = l_{g3} = l_g$, we find

$$k_a = \frac{\partial F_a}{\partial z} \cong \frac{3\mu_0 A E_m^2}{4l_g^3}\frac{1+\alpha_1-\alpha_0}{1+\alpha_1+\alpha_2} \qquad (>0) \tag{9}$$

In this type of magnetic bearing, the attractive force reacting between the magnetic poles of the rotor and the stator results in the passive stabilization. No estimating methods of bearing radial stiffness can be compared with Roters' method. Therefore, we applied numerical simulation of the magnetic field to estimate the radial stiffness. Figure 2 shows an example of the computation result representing the magnetic field in the vicinity of a gap. The successive method of accelerating relaxation (SOR) is applied to solve the two-dimensional Laplace equation $\nabla^2 u = 0$ (where u is the magnetic potential) under suitable boundary conditions. The magnetic flux line Φ_{r1}, which emanates from the stator counter-surface to the rotor pole and terminates in the upper surface of the rotor, contributes to the radial restoring force. Another magnetic flux line Φ_{r2}, which emanates from the rotor counter-surface of the stator, also contributes to the radial restoring force. Assuming B_{r1} is the magnetic flux density resulting from Φ_{r1} and B_{r2} is that from Φ_{r2}, the radial restoring force f_r per unit peripheral length is expressed as

$$f_r = \frac{1}{2\mu_0}\left(\int_{l_1} B_{r_1}^2\,\mathrm{d}l + \int_{l_2} B_{r_2}^2\,\mathrm{d}l\right) \tag{10}$$

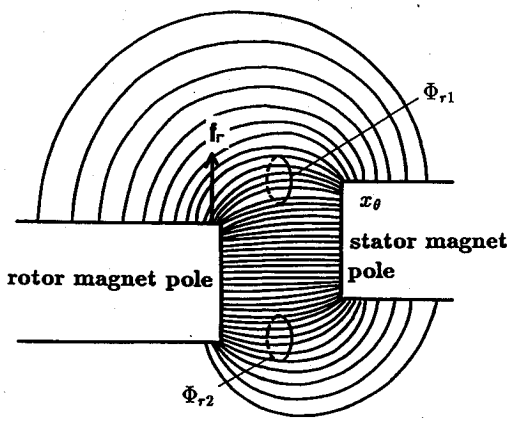

Fig. 2 Magnetic field and restoring force in the vicinity of gap.

where l_1 is the path along the upper surface and l_2 is that along the lower surface. Assuming the eccentricity of the rotor relative to the center of the stator is x, the relative radial displacement x_θ depends on the peripheral angle θ. Then, the total radial restoring force F_r is obtained by integrating $f_r(\theta)$ along the peripheral angle from 0 to 2π, i.e.,

$$F_r = 2\int_0^{2\pi} \pi f_r(\theta) r_m\,\mathrm{d}\theta \tag{11}$$

where r_m is the mean radius of the stator pole. The radial bearing stiffness $k_r = \partial F_r/\partial x$ was estimated on our example as

$$k_r \simeq \left(\frac{1}{16}\sim\frac{1}{14}\right)k_a \tag{12}$$

Analysis

The design technique for a high bearing stiffness was discussed in the preceding section. The means for realizing a high rotational speed of the rotor are investigated in the following sections.

Modeling

By using the earlier results and dynamics we can model rotor whirling motion. The rotor is suspended by the magnetic bearing and can move without contact within the gap clearance of the bearing. The rotor structural stiffness is assumed high enough for it to be treated as a rigid body. Then rotor motion may be separated into a translational mode and a tilting mode. Essential features of the dynamic behavior can be deduced from the translational mode as far as the rotor motion is concerned. When the tilting mode is treated, the interaction between the satellite carrying the wheel should be taken into consideration.[8] The tilting motion is dropped in the following sections. (The damping characteristics in the passively stabilized axis mentioned earlier can be deduced with only the translational mode motion.) Figure 3a schematically shows the longitudinal cross-sectional view of the outer rotor and the inner stator. The stator is deflected elastically in the radial directions in an eccentric manner (z axis is defined in the vertical direction). This figure schematically shows only the radial motion of the rotor. The coils are not shown in the figure. Figure 3b shows the horizontal cross-sectional view of the bearing stator and the rotor featuring the motion of their center. The stator cross section in this figure is assumed to represent the mean position of its upper cross section and its lower cross section. The stator center point is at (ξ,η) due to

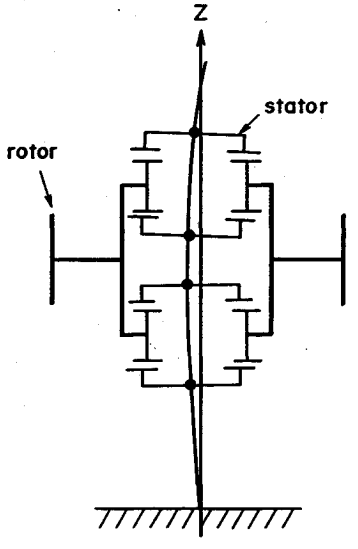

Fig. 3a Schematics of longitudinal cross-sectional view of wheel.

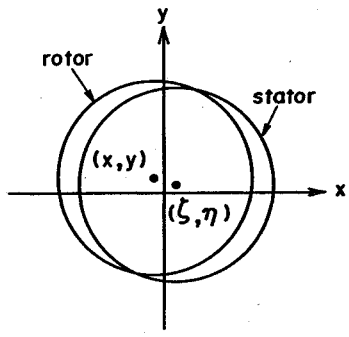

Fig. 3b Position of center of rotor and stator in transverse cross section.

elastic deformation from its nominal position. The rotor center point at (x,y) is displaced due to its whirling motion. The equations of motion for the rotor center of the mass are

$$\ddot{x} + \omega_0^2 x + 2\delta_{ot}\dot{x} + 2\delta_{it}(\dot{x} + \omega y) + \alpha\xi = 0 \tag{13a}$$

$$\ddot{y} + \omega_0^2 y + 2\delta_{ot}\dot{y} + 2\delta_{it}(\dot{y} - \omega x) + \alpha\eta = 0 \tag{13b}$$

where $\dot{x}$, $\dot{y}$, $\ddot{x}$, and $\ddot{y}$ are the first and second derivatives of x and y with time, respectively; other symbols are defined as follows: ω is the angular speed of rotor, ω_0 the critical speed of rotor caused by finite bearing stiffness, δ_{ot} the damping factor due to eddy current loss in the stator, δ_{it} the damping factor due to eddy current loss in the rotor, and α the reaction factor due to stator deflection. The terms δ_{it} and δ_{ot} represent electromagnetic induction effect related with the relative speed between the rotor and stator. The terms $2\delta_{it}\omega y$ in Eq. (13a) and $-2\delta_{it}\omega x$ in Eq. (13b) represent the coupling effect where an eccentricity in the one axis induces another eccentricity in the other axis due to the rotation. Their effect will be re-examined later in more detail. The terms $\alpha\xi$ in Eq. (13a) and $\alpha\eta$ in Eq. (13b) represent the coupling effect between the rotor and the stator due to the eccentricity. The equations of the stator motion at its center of mass are described as

$$\ddot{\xi} + \omega_{rx}^2\xi + 2\delta_r\dot{\xi} + \alpha' x = 0 \tag{14a}$$

$$\ddot{\eta} + \omega_{ry}^2\eta + 2\delta_r\dot{\eta} + \alpha' y = 0 \tag{14b}$$

where $\dot{\xi}$, $\ddot{\xi}$, $\dot{\eta}$, and $\ddot{\eta}$ are the first and second derivatives of ξ and η with time, respectively, and the other symbols are defined as follows: ω_{rx} and ω_{ry} are the mode angular speeds of the stator along the x and y axes due to its structural elasticity, δ_r the damping factor of the stator due to its elastic deflection, and α' the reaction factor due to the rotor eccentricity. The terms ω_{rx} and ω_{ry} are distinctive to each other to prepare for the introduction of the anisotropy of the structural stiffness in the stator. The anisotropy of the structural stiffness will turn out later to be equivalent to that of the bearing stiffness. The terms $\alpha' x$ and $\alpha' y$ represent the radial restoring force effect, as mentioned in the preceding section, due to the rotor displacement. Equations (13a–14b) describe the motion of the rotor and the stator considering the anisotropy of the stator structural stiffness.

Damping Factor of Isotropic Bearing Rotor

Taking the stiffness of stator as infinite, Eqs. (14) are discarded, and $\xi = \eta = 0$ is assumed in Eqs. (13). The remaining equations represent the motion of the rotor suspended by isotropic bearing:

$$\ddot{x} + \omega_0 2x + 2(\delta_{ot} + \delta_{it})\dot{x} + 2\delta_{it}\omega y = 0 \tag{15a}$$

$$\ddot{y} + \omega_0 2y + 2(\delta_{ot} + \delta_{it})\dot{y} - 2\delta_{it}\omega x = 0 \tag{15b}$$

The coupling effects are expressed explicitly in the last terms in Eqs. (15a) and (15b). To obtain an approximate solution for the dynamic characteristics of the rotor, the method of averaging is applied as follows, transferring the variables x and y to the harmonic functions of ω_0:

$$x = ae^{i\omega_0 t} + a^* e^{-i\omega_0 t}, \qquad y = be^{i\omega_0 t} + b^* e^{-i\omega_0 t} \tag{16}$$

where a^* and b^* are the conjugate complex variables of a and b, respectively. Inserting Eq. (16) into Eqs. (15a) and (15b) we obtain the following equations:

$$\begin{aligned}&\ddot{a}e^{i\omega_0 t} + \ddot{a}^* e^{-i\omega_0 t} + 2i\omega_0(\dot{a}e^{i\omega_0 t} - \dot{a}^* e^{-i\omega_0 t})\\ &+ 2(\delta_{ot} + \delta_{it})(\dot{a}e^{i\omega_0 t} + \dot{a}^* e^{-i\omega_0 t}) + i\omega_0(ae^{i\omega_0 t} - a^* e^{-i\omega_0 t})\\ &+ 2\sigma_{it}\omega(be^{i\omega_0 t} + b^* e^{-i\omega_0 t}) = 0\end{aligned} \tag{17a}$$

$$\begin{aligned}&\ddot{b}e^{i\omega_0 t} + \ddot{b}^* e^{-i\omega_0 t} + 2i\omega_0(\dot{b}e^{i\omega_0 t} - \dot{b}^* e^{-i\omega_0 t})\\ &+ 2(\delta_{ot} + \delta_{it})(\dot{b}e^{i\omega_0 t} + \dot{b}^* e^{-i\omega_0 t})\\ &+ i\omega_0(be^{i\omega_0 t} - b^* e^{-i\omega_0 t}) + 2\delta_{it}\omega(ae^{i\omega_0 t} + a^* e^{-i\omega_0 t}) = 0\end{aligned} \tag{17b}$$

Neglecting $\ddot{a}$, $\ddot{a}^*$, and the other higher-order terms, we obtain the following equations by multiplying the remaining terms by $e^{-i\omega_0 t}$:

$$\dot{a} = (\delta_{ot} + \delta_{it})a + i\delta_{it}(\omega/\omega_0)b + f_1(\dot{a}^*, a^*, b^*)e^{-2\omega_0 t} \tag{18a}$$

$$\dot{b} = (\delta_{ot} + \delta_{it})b - i\delta_{it}(\omega/\omega_0)a + f_2(\dot{b}^*, b^*, a^*)e^{-2\omega_0 t} \tag{18b}$$

where f_1 and f_2 are the linear functions of $\dot{a}^*$, a^*, b^*, and $\dot{b}^*$, b^*, a^*, respectively. The third terms on the right sides of Eqs. (18) are of the same order magnitude. The sinusiodal functions have frequency $2\omega_0$. When focusing the slow variation of $\dot{a}$ and $\dot{b}$, we can eliminate the last terms by averaging them over the period (π/ω_0). This approximation is valid for the frequency below (ω_0/π). Then we obtain the following equations, which approximate Eqs. (18):

$$\dot{a} - (\delta_{ot} + \delta_{it})a - i\delta_{it}(\omega/\omega_0)b = 0 \tag{19a}$$

$$\dot{b} - (\delta_{ot} - \delta_{it})b + i\delta_{it}(\omega/\omega_0)a = 0 \tag{19b}$$

Equations (19) form a set of simultaneous, ordinary differential equations with constant coefficients. We obtain the real part δ_0 of the eigenvalue of the system as

$$\delta_0 = (\delta_{ot} + \delta_{it}) \pm \delta_{it}(\omega/\omega_0) \tag{20}$$

The imaginary parts of the eigenvalues are assumed to be $\pm\omega_0$, because using them in Eqs. (17) and then Eq. (20) represents the damping factor. From the equation, it is found that the lower value of the damping factor decreases with the angular speed of rotor ω and it becomes negative beyond the boundary speed at which the right side becomes zero. Accordingly, the limiting speed ω_c of the rotor stabilization is expressed as

$$\omega_c = (\delta_{ot} + \delta_{it})(\omega_0/\delta_{it}) \tag{21}$$

This equation shows that the internal loss δ_{it} causes a decrease in the limiting speed ω_c. To increase value ω_c, we must increase ω_0 or decrease δ_{it}, because as a practical matter we cannot decrease δ_{it} below some minimum value.

Modification of Damping Factor

Equation (20) has been deduced on the assumption of isotropic bearing stiffness. The reason δ_0 decreases with ω is because the isotropy of bearing stiffness helps the growth of rotor whirling motion through a tight coupling effect between

x and y degrees of freedom of the motion, and rotational energy of rotor is poured to the whirling motion. It is pointed out that the anisotropy of bearing stiffness prevents the internal loss factor from decreasing the mode damping factor.[4] We formulate this effect from Eqs. (13a–14b). Now, we transfer ξ to the following equation focusing on Eq. (14a).

$$\xi = ce^{i\omega_0 t} + c^* e^{-i\omega_0 t} \tag{22}$$

Inserting Eq. (22) into Eq. (14a), we can obtain the following relation about c after neglecting the derivatives of c:

$$c = \frac{\alpha'}{(\omega_{rx}^2 - \omega_0^2) + i2\omega\delta_r} a \tag{23}$$

Using Eq. (23) in Eq. (22), and also Eq. (16), after neglecting the derivatives of a, we can obtain the following expression:

$$\xi = -\frac{\alpha'}{\omega_{rx}^2 - \omega_0^2} x + \frac{2\alpha'\delta_r}{(\omega_{rx}^2 - \omega_0^2)^2}\dot{x} \tag{24}$$

After introducing Eq. (29) into Eq. (13a), we finally obtain

$$\ddot{x} + \left(\omega_0^2 - \frac{\alpha\alpha'}{\omega_{rx}^2 - \omega_0^2}\right)x + 2\left[\delta_{ot} + \frac{\alpha\alpha'\delta r}{(\omega_{rx}^2 - \omega_0^2)^2}\dot{x} + 2\delta_{it}(\dot{x} + \omega y)\right] = 0 \tag{25}$$

To compare the factors in this equation with the corresponding factors in Eq. (13a), we must modify ω_0 and δ_{ot} as follows:

$$\Delta\omega_{0x} = -\frac{\alpha\alpha'}{2\omega_0(\omega_{rx}^2 - \omega_0^2)} \tag{26}$$

$$\Delta\omega_{otx} = -\frac{\alpha\alpha'\delta_r}{(\omega_{rx}^2 - \omega_0^2)^2} \tag{27}$$

The modification on $\Delta\omega_{0y}$ and $\Delta\delta_{oty}$ should be made as

$$\Delta\omega_{0y} = -\frac{\alpha\alpha'}{2\omega_0(\omega_{ry}^2 - \omega_0^2)} \tag{28}$$

$$\Delta\delta_{oty} = \frac{\alpha\alpha'\delta_r}{(\omega_{ry}^2 - \omega_0^2)^2} \tag{29}$$

The modification of $\Delta\delta_{otx}$ and $\Delta\delta_{oty}$ is practically negligible, because δ_r cannot be large. The anisotropy of structural stiffness in the stator can be transferred accordingly into that of the bearing stiffness. So, we replace ω_0 with ω_{0x} and ω_{0y} as follows:

$$\omega_{0x} = \omega_0 + \Delta\delta_{0x} \tag{30a}$$

$$\omega_{0y} = \omega_0 + \Delta\delta_{0y} \tag{30b}$$

Now, we should return to Eqs. (15a) and (15b). The following equations express the modified equations of the rotor motion considering the anisotropy of bearing stiffness caused by structural anisotropy:

$$\ddot{x} + \omega_{0x}^2 x + 2(\delta_{ot} + \delta_{it})\dot{x} + 2\delta_{it}\omega y = 0 \tag{31a}$$

$$\ddot{y} + \omega_{0y}^2 x + 2(\delta_{ot} + \delta_{it})\dot{y} - 2\delta_{it}\omega x = 0 \tag{31b}$$

The transfer of the variables x and y with the harmonic function of the angular speed ω_{0x} is executed the same way as in Eqs. (18),

$$x = ae^{i\omega_{0x}t} + a^* e^{-i\omega_{0x}t}, \qquad y = be^{i\omega_{0y}t} + b^* e^{-i\omega_{0y}t} \tag{32}$$

After applying the method of averaging to Eqs. (31), we obtain the following equations relating a and b,

$$\dot{a} + (\delta_{ot} + \delta_{it})a - i\left(\frac{\omega}{\omega_{0x}}\right)\delta_{it}b = 0 \tag{33a}$$

$$\dot{b} + [i\Delta - (\delta_{ot} + \delta_{it})]b + i\left(\frac{\omega}{\omega_{0x}}\right)\delta_{it}a = 0 \tag{33b}$$

where

$$\Delta = (\omega_{0y} - \omega_{0x})/2\omega_{0x} \tag{34}$$

The real part of the eigen solution of the equations, that is the damping factor δ_0, is modified as follows:

$$\Delta > 2\delta_{it}\left(\frac{\omega}{\omega_{0x}}\right), \qquad \delta_0 = \delta_{ot} + \delta_{it} \tag{35}$$

$$\Delta \le 2\delta_{it}\left(\frac{\omega}{\omega_{0x}}\right), \qquad \delta_0 = \delta_{ot} + \delta_{it} \pm \left[\delta_{it}^2 + \left(\frac{\omega}{\omega_{0x}}\right)^2\right]^{1/2} \tag{36}$$

These relations are shown in Fig. 4, where the dotted line represents Eq. (20) and the solid line Eqs. (35) and (36). It is readily apparent that the improvement of the damping factor is significant. The limiting speed of the rotor ω_c increases markedly as shown in the following equation:

$$\omega_c = \left[(\delta_{ot} + \delta_{it})^2 + \left(\frac{\Delta}{2}\right)^2\right]^{1/2}\left(\frac{\omega_{0x}}{\delta_{it}}\right) \tag{37}$$

This equation implies that remarkable improvement of ω_c is attained if the difference of the structural stiffness of the stator in the two transverse axes, as given by

$$\Delta = (\omega_{0y} + \omega_{0x})/2\omega_{0x} \tag{38}$$

is significant.

Experiment

To test the analysis developed, the experiment was conducted using the model shown in Fig. 1a. The model is contained in a vacuum chamber with air pressure of 3 Torr, as shown in Fig. 5. The rotor radial motion is detected by the position sensors located close to the lower end of the rotor. The damping factor of the system is measured by the sensors immediately after an impulse is given on the vacuum chamber. Figure 6a shows an example of the damping spectrum curve of the translational motion measured on the wheel of the isotropic stiffness at rotational speed 0. The curve was reduced by transferring the vibration signal into the amplitude spectrum through the fast Fourier transformer (FFT). The critical frequency of the wheel is 28 Hz. The Q value reduced to the

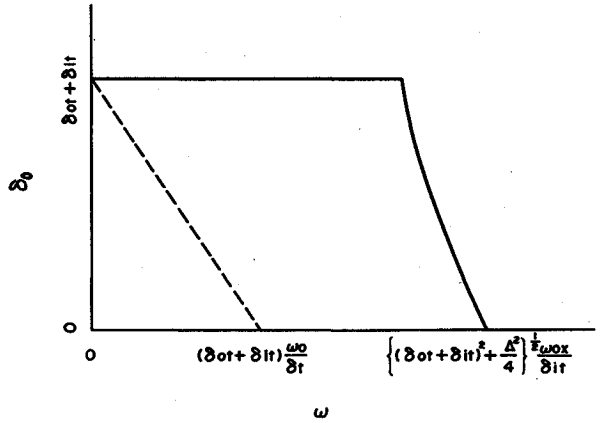

Fig. 4 Damping factor variation with rotational speed.

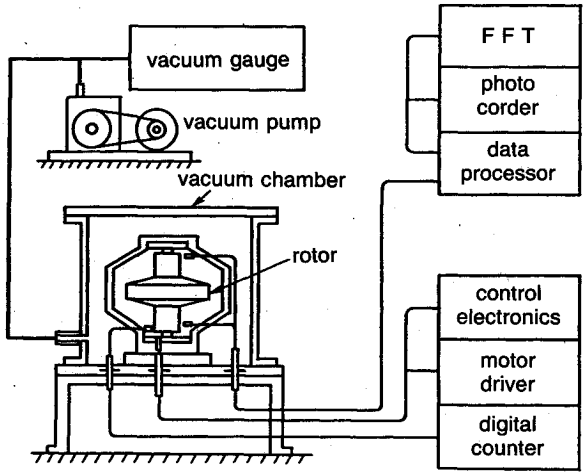

Fig. 5 Schematics of experimental setup.

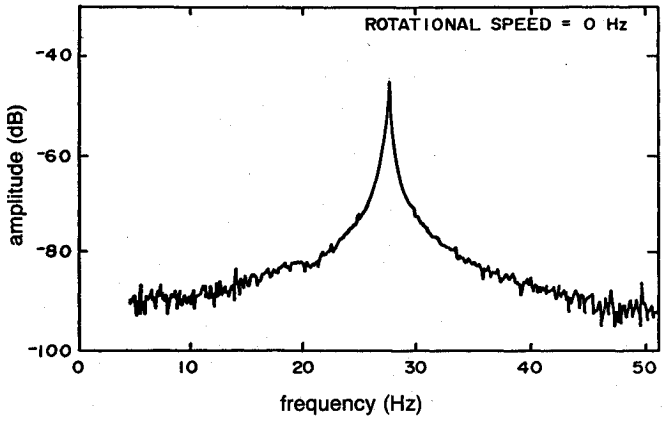

a) Rotational speed 0 Hz

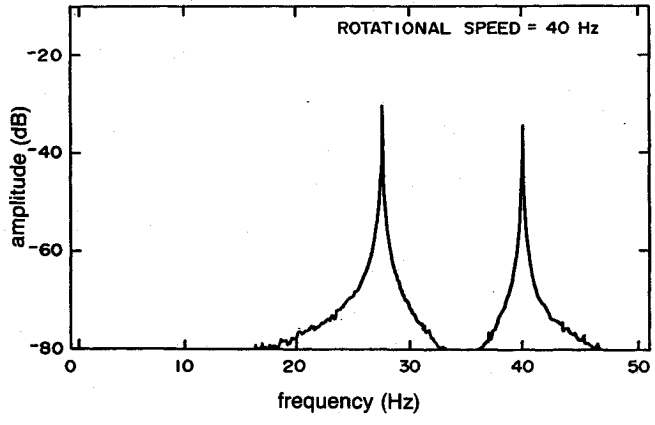

b) Rotational speed 40 Hz

Fig. 6 Damping spectrum curve of translational mode motion.

damping factor is obtained from the spectrum curve centered at 28 Hz. Figure 6b shows another example of the damping spectrum curve of the same mode at rotational speed 40 rps. We can find two peaks; one at 28 Hz and the other at 40 Hz identified with the rotational speed. The curve centered at 28 Hz has become sharper compared with the curve at rotational speed 0. This means that the damping factor at rotational speed 40 Hz is less than that at 0 Hz. The result of the measurement in the case of the stator with isotropic stiffness is

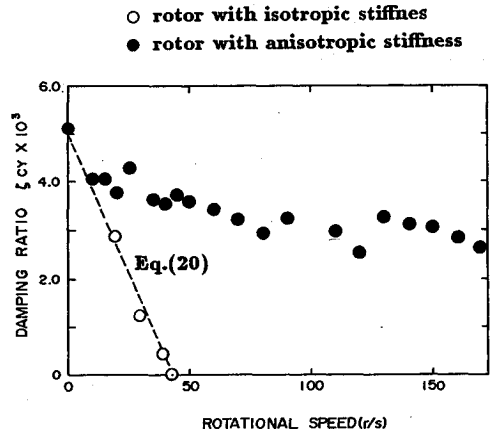

Fig. 7 Damping ratio variation of the rotor with the rotational speed.

shown in Fig. 7. The white circles represent the measured damping ratio $\eta_{cy}(=\delta_0/\omega_0)$. From the estimated curve in the figure, the limiting frequency $f_c(=\omega_c/2\pi)$ is figured as 43 Hz.

One of the effective measures of improving the limiting speed is to increase δ_{it}. Accordingly, we decreased the stiffness of the inner stator, intending the increase of the dissipation energy caused by elastic deflection. Another effective measure is to utilize the anisotropic structural stiffness of the inner stator. A small key groove was dug on an end of the center shaft, which is the main member of the inner stator. Finally, the following characteristics were measured:

$$\begin{aligned} \omega_0 &= 176 \text{ rad/s} \quad (28 \text{ Hz}) \\ \omega_{rx} &= 230 \text{ rad/s} \\ \omega_{ry} &= 274 \text{ rad/s} \\ \alpha\alpha' &= 3 \times 10^6 \text{ s}^{-4} \\ \delta_{ot} + \delta_{it} &= 0.88 \text{ s}^{-1} \end{aligned}$$

The estimated limiting speed based on the preceding characteristics is

$$\omega_c = 2.49 \times 10^3 \text{ rad/s} \quad (= 397 \text{ rps}) \tag{39}$$

The experimental results that support the estimation procedure were shown also in Fig. 7. The black circles represent the measured damping ratio of the stator with the anisotropic stiffness. There is remarkable improvement of the damping characteristics, although the adequacy of Eq. (39) is not clear for lack of the experimental data above the rotational speed of 170 (r/s).

Conclusion

A method for determining the effects of the stiffness of the magnetic bearing supporting a rotor have been developed, which incorporates active stabilization in the axial direction and passive stabilization in the two orthogonal radial directions. An analytical expression for the damping characteristics of the rotor was deduced. From this expression it was concluded that the anisotropic stiffness of the stator structure can be used effectively to improve the passive damping characteristics. The prediction of the improved damping characteristics was verified experimentally.

Acknowledgment

The authors wish to thank S. Hagihara and K. Yabu-uchi of Mitsubishi Electric Corporation and O. Okamoto and T. Kida of the National Aerospace Laboratory. They enthusiastically cooperated with the authors during both the analytical study and the experiment.

References

[1]Kamerbeek, E. M. H., "Magnetic Bearing," *Philips Technical Review*, Vol. 41, No. 11/12, 1983/84, pp. 348–361.

[2]Poubeau, P. C., "Satellite Flywheels with Magnetic Bearings and Passive Radial Centering," *Journal of Spacecraft and Rockets*, Vol. 17, No. 2, 1980, pp. 93–100.

[3]Knorrchen, H., and Lange, T., "Modular Design and Dynamic Tests on Active Bearing Momentum Wheel," IFAC-ESA Joint Symposium on Automatic Control in Space, Noordwijkerhout, July 1982.

[4]Gasch, R., and Pfutzner, H., *Rotordynamik, Eine Einfuhrung*, Spinger-Verlag, Berlin, Germany, 1975.

[5]Kawamoto, H., "Stiffness Analysis of Magnetic Bearing," *Transaction of the Japan Society of Mechanical Engineering (Ser.C)*, Vol. 48, No. 427, 1982, pp. 367–372 (in Japanese).

[6]Sabnis, A. V., et al., "A Magnetically Suspended Large Momentum Wheel," *Journal of Spacecraft and Rockets*, Vol. 12, No. 7, 1975, pp. 420–426.

[7]Roters, H. C., *Electromagnetic Devices*, Wiley, New York, 1941.

[8]Inoue, M., Tsuchiya, K., Nakajima, A., and Murakami, C., "Nutation Stability of a Satellite Equipped with an Active Magnetic Momentum Wheel," *Journal of Space Technology and Science*, Vol. 3, Feb. 1988, pp. 127–136.